JOURNAL OF GEOPHYSICAL RESEARCH: SOLID EARTH, VOL. 118, 4729–4744, doi:10.1002/jgrb.50343, 2013

Dielectric relaxation behavior of Callovo-Oxfordian clay rock: A hydraulic-mechanical-electromagnetic coupling approach

Norman Wagner,[1] Thierry Bore,[2] Jean-Charles Robinet,[2] Daniel Coelho,[2] Frederic Taillade,[3] and Sylvie Delepine-Lesoille[2]

Received 24 April 2013; revised 9 August 2013; accepted 12 August 2013; published 16 September 2013.

[1] Water content is a key parameter to monitor in nuclear waste repositories such as the planed underground repository in Bure, France, in the Callovo-Oxfordian (COx) clay formation. High-frequency electromagnetic (HF-EM) measurement techniques, i.e., time or frequency domain reflectometry, offer useful tools for quantitative estimation of water content in porous media. However, despite the efficiency of HF-EM methods, the relationship between water content and dielectric material properties needs to be characterized. Moreover, the high amount of swelling clay in the COx clay leads to dielectric relaxation effects which induce strong dispersion coupled with high absorption of EM waves. Against this background, the dielectric relaxation behavior of the clay rock was studied at frequencies from 1 MHz to 10 GHz with network analyzer technique in combination with coaxial transmission line cells. For this purpose, undisturbed and disturbed clay rock samples were conditioned to achieve a water saturation range from 0.16 to nearly saturation. The relaxation behavior was quantified based on a generalized fractional relaxation model under consideration of an apparent direct current conductivity assuming three relaxation processes: a high-frequency water process and two interface processes which are related to interactions between the aqueous pore solution and mineral particles (adsorbed/hydrated water relaxation, counter ion relaxation and Maxwell-Wagner effects). The frequency-dependent HF-EM properties were further modeled based on a novel hydraulic-mechanical-electromagnetic coupling approach developed for soils. The results show the potential of HF-EM techniques for quantitative monitoring of the hydraulic state in underground repositories in clay formations.

Citation: Wagner, N., T. Bore, J.-C. Robinet, D. Coelho, F. Taillade, and S. Delepine-Lesoille (2013), Dielectric relaxation behavior of Callovo-Oxfordian clay rock: A hydraulic-mechanical-electromagnetic coupling approach, *J. Geophys. Res. Solid Earth*, *118*, 4729–4744, doi:10.1002/jgrb.50343.

1. Introduction

[2] Safety solutions of management for all radioactive waste in order to protect the present and future generations from the waste risks is an essential need. The French National Radioactive Waste Management Agency (ANDRA; Agence nationale pour la gestion des dèchets radioactifs) is in charge of long-term management of radioactive waste produced in France. ANDRA has systematically studied the possibility of implementing an underground repository for high-level and long-lived waste in the underground laboratory (URL) in Bure, France (Meuse district, eastern Paris Basin, France), built during the early 2000s [*Delay et al.*, 2008]. The geological formation under consideration consists of a 130 m thick clay rock layer located at a depth of 500 m [*Linard et al.*, 2011]. The water content is a key state parameter for monitoring and prediction of thermal, hydraulic, mechanical, chemical, and radiological (THMCR) processes in nuclear waste repositories since it drives radioactivity confinement. More precisely, monitoring water content in the Callovo-Oxfordian clay, host rock of the planed underground repository, enables to confirm and precise long-term radionuclide transfer models.

[3] Unlike mechanical and thermal processes for which vibrating wire sensors and platinum probes have proved their efficiency for more than half a century on dam monitoring, for water content monitoring, very few technologies allow accurate and long-term monitoring without maintenance. The success of quantitative water content estimation in porous media with high-frequency (radio and microwave) noninvasive and minimal invasive electromagnetic (HF-EM) measurement techniques is caused by the dipolar character of the water molecules resulting in a high permittivity

[1]Institute of Material Research and Testing, Bauhaus-Universität Weimar, Weimar, Germany.
[2]French National Radioactive Waste Management Agency, Paris, France.
[3]French Institute of Science and Technology of Transport, Development, and Network, Université Paris Est, Paris, France.

Corresponding author: N. Wagner, Institute of Material Research and Testing, Bauhaus-Universität Weimar, Coudraystraße 4, 99423, Weimar, Germany. (norman.wagner@mfpa.de)

2169-9313/13/10.1002/jgrb.50343

in comparison to other phases such as solid particles or gas inclusions [*Hoekstra and Delaney*, 1974; *Topp et al.*, 1980]. However, interactions between an aqueous pore solution and solid phases lead to strong contributions to the dielectric material properties due to interphase processes [*Ishida et al.*, 2000, 2003; *Wagner and Scheuermann*, 2009]. Therefore, the dielectric relaxation behavior contains additional information, besides the volume fraction of free pore water, about the structure and dynamics of water in the porous material, especially in clays [*Bergman and Swenson*, 2000; *Ryabov et al.*, 2001]. Against this background, high-frequency electromagnetic (HF-EM) measurement techniques such as time or frequency domain reflectometry (TDR, FDR) offer the possibility to obtain physicochemical properties of porous media noninvasive/minimal invasive with high spatial and temporal resolution [*Robinson et al.*, 2003]. ANDRA initiated tests on water content sensing chains in 1994, when a one-to-one scale mock-up of a cover structure, made of crushed clay, was instrumented with four water-content sensor types. Capacitive sensors, time domain reflectometry (TDR) sensors, tensiometric suction probes, and neutronic probes were implemented. TDR resulted to be the only efficient technology: It is long-time stable and provides accurate measurements. Currently, more than 80 TDR sensors still provide accurate water-content measurements. However, despite the efficiency, TDR actually provides indirect measurement of water content. A major difficulty to face is the link between the performed permittivity measurements with host material water content to sense. Various empirical models are used for soil [*Topp et al.*, 1980; *Dobson et al.*, 1985; *Hallikainen et al.*, 1985; *Robinson et al.*, 2003], which are mostly not simply transferable to soils with a high content of swelling clay minerals [*Kelleners et al.*, 2005; *Robinson et al.*, 2005; *Kupfer et al.*, 2007; *Wagner et al.*, 2007a; *Schwartz et al.*, 2009]. Another solution is to rely on laboratory calibrations. However, it encounters opposite specifications (i) the need for large samples to place the TDR probes with respect the electromagnetic interaction field and (ii) the duration of water-content-forced variations in the sample. Hence, there is a need of broadband electromagnetic characterization of clay rocks under defined THMCR conditions.

[4] Concerning the clay rock, ANDRA has performed a huge number of physical and chemical measurements in its underground research laboratory, located at Bure [*Sammartino et al.*, 2003; *Gaucher et al.*, 2004; *Jougnot et al.*, 2010a; *Okay et al.*, 2013]. However, the electromagnetic properties and especially the dielectrical permittivity remain poorly known. A campaign of characterization has been reported on the clay from the Mont Terri (Switzerland) site with a coaxial transmission line. For ease of manipulation, the study only considered crushed and altered clay. Samples were crushed down to 2 mm grains and recompacted. Such a preparation modifies initial clay structure (porosity, pore size distribution). Thus, the representativeness of permittivity measurements obtained on crushed clay compared to the unaltered rock is restricted. Electromagnetic properties of Bure Callovo-Oxfordian clay rock were also measured with three different methods: in the low-frequency range (from 10 mHz to 45 kHz) with spectral-induced polarization [*Jougnot et al.*, 2010b], the intermediate range (from 100 kHz to 10 MHz) using impedance measurement, and at higher-frequency range (from 500 MHz to 10 GHz) with an open-ended coaxial probe [*Comparon*, 2005]. However, a large part of the useful dielectric spectrum is missing. Standard TDR devices (such as Campbell TDR100) make use of a broadband step voltage pulse with a bandwidth from about 20 kHz to roughly 1.5 GHz [*Heimovaara et al.*, 1994].

[5] Typically, in the frequency range from 100 Hz to at least 200 MHz capacitance methods are used to determine dielectric spectra [*Kremer*, 2003; *Kaatze and Feldman*, 2006]. The most familiar and simple geometry is the parallel-plate configuration [*Salat and Junge*, 2010; *Wagner et al.*, 2011a]. With such cells, the specimen is sandwiched between two parallel arranged electrodes and the dielectric spectra are derived from the measured capacitance and dissipation factor. The measurement requires a crushed sample with particle size <2 mm and placing small sample volumes in the cell which destroys the natural structure. In the frequency range from 1 MHz to 10 GHz, time or frequency domain coaxial transmission line or open-ended coaxial line techniques are used [e.g., *Behari*, 2005; *Oswald et al.*, 2006; *Arcone et al.*, 2008; *Wagner et al.*, 2011a]. Especially open-ended coaxial probes are popular for dielectric characterization because of their broadband capabilities and almost nondestructive functioning [*Wagner et al.*, 2011b]. Their application to explore soil permittivity is presented in *Skierucha et al.* [2004], *Kelleners et al.* [2005], *Chen and Or* [2006], *Wagner et al.* [2007c], and *Wagner et al.* [2011a]. To obtain the dielectric properties of the material, the open-ended coaxial probe is simply pressed against the sample and the complex reflection coefficient (S_{11}) is measured and converted to complex permittivity by means of a lumped-element equivalent circuit [*Wagner et al.*, 2013]. Accurate permittivity measurements require a close contact between the material under test and the probe. Air gaps caused by surface roughness of the samples affect the measurement quality [*Comparon*, 2005]. Consequently, the open-ended coaxial probe method is more suited for liquids and homogeneous fine-grained materials than for hard rock samples. Studies by *Folgero* [1998], *Shang et al.* [1999], *Rowe et al.* [2001], *Oswald et al.* [2006], *Wagner et al.* [2011a], *Siggins et al.* [2011], and *Bohleber et al.* [2012] describe two-port coaxial transmission line technique to investigate complex permittivity of soil. In *Lauer et al.* [2012], a new technique was introduced to measure broadband dielectric spectra of undisturbed samples which was extended in *Wagner and Lauer* [2012] to simultaneously determine the dielectric relaxation behavior and soil water characteristic curve.

[6] In this study, the dielectric relaxation behavior of the Callovo-Oxfordian clay rock was studied in the frequency range from at least 1 MHz to 10 GHz at atmospheric conditions with network analyzer technique in combination with coaxial transmission line cells. For this purpose, undisturbed and disturbed clay-rock samples were prepared as cylinders and conditioned at defined relative humidity between 10% and nearly 100% over saturated salt solutions as well as distilled water to achieve a water saturation range from at least 0.16 to nearly saturation. The relaxation behavior was quantified based on a broadband generalized fractional relaxation model under consideration of an apparent direct current contribution assuming three relaxation processes: a high-frequency water process and two interface processes which

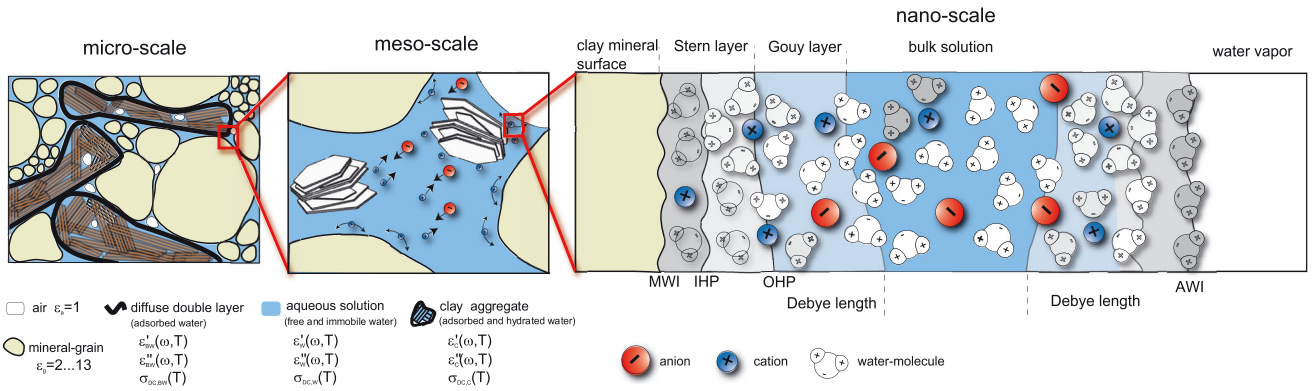

Figure 1. Simplified schematic illustration of the structure of a porous mineral material at different spatial scales with indication of contributions of the single phases (mineral particles, aqueous solution with water in different binding states and ions in the pore solution as well as air) to the electromagnetic material properties. MWI/AWI is mineral-water or air-water interface, IHP/OHP is inner or outer Helmholtz plane [*Iwata et al.*, 1995; *Jougnot et al.*, 2010b; *Wagner and Scheuermann*, 2009; *Leroy et al.*, 2012].

are related to interactions between the aqueous pore solution and mineral particles such as adsorbed and hydrated water relaxation superposed with counter ion relaxation processes and Maxwell-Wagner effects. The frequency-dependent HF-EM properties were further modeled based on a novel hydraulic-electromagnetic coupling approach developed for soils under consideration of the water sorption isotherm as well as structural changes due to swelling effects.

2. Dielectric Relaxation Behavior

[7] In general, the complex permittivity of partially saturated porous mineral material depends on the high-frequency electromagnetic (HF-EM) properties of the appropriate solid phases (texture, mineralogy), their interaction with water vapor and aqueous solutions as well as soil structure (density, particle shape distribution, see *Wagner et al.* [2011a] and *Wagner and Scheuermann* [2009], see Figure 1).

[8] Based on Maxwell's equations of electrodynamics, broadband electromagnetic transfer functions of a porous mineral material can be defined in terms of complex relative effective permittivity

$$\varepsilon^{\star}_{r,\mathrm{eff}}(\omega,T,p,\ldots)=\frac{\varepsilon^{\star}_{\mathrm{eff}}(\omega,T,p,\ldots)}{\varepsilon_0} \tag{1}$$

or effective conductivity

$$\sigma^{\star}_{\mathrm{eff}}(\omega,T,p,\ldots)=j\omega\varepsilon^{\star}_{\mathrm{eff}}(\omega,T,p,\ldots) \tag{2}$$

and complex relative effective magnetic permeability

$$\mu^{\star}_{r,\mathrm{eff}}(\omega,T,p,\ldots)=\frac{\mu^{\star}_{\mathrm{eff}}(\omega,T,p,\ldots)}{\mu_0} \tag{3}$$

with imaginary unit $j=\sqrt{-1}$, angular frequency $\omega=2\pi f$, as well as permittivity ε_0 and magnetic permeability μ_0 of free space. The transfer functions depend on frequency as well as on the thermodynamic state parameters such as temperature T, fluid pressure p, and stress-strain state [*Hoekstra and Delaney*, 1974; *Jonscher*, 1977; *Schoen*, 1996; *Santamarina et al.*, 2001; *Börner*, 2006; *Stillman and Olhoeft*, 2008]. In this study, the selected clay-rock samples justify the assumption that magnetic effects can be neglected so here $\mu^{\star}_{r,\mathrm{eff}}$ will not be discussed (see section 3.2). Equations (1) and (2) can be defined based on the concept of an intrinsic complex electrical permittivity $\varepsilon^{\star}$ or conductivity $\sigma^{\star}$ of the material [*Wagner et al.*, 2007b]. Moreover, to relate the complex transfer functions to measurable quantities with HF-EM techniques such as TDR, ground penetrating radar (GPR), or electrical resistivity tomography (ERT), it is reasonable to define additional real effective conductivity and a real effective relative permittivity [see *Katsube and Collet*, *Katsube and Collet*; *Jonscher*, 1977; *Jonscher*, 1983; *Wagner et al.*, 2011a]:

$$\varepsilon_{r,\mathrm{eff}}(\omega)=\frac{\varepsilon'_{\mathrm{eff}}(\omega)}{\varepsilon_0}=\varepsilon'_r(\omega)+\frac{\sigma''(\omega)}{\varepsilon_0\omega}, \tag{4}$$

$$\sigma_{\mathrm{eff}}(\omega)=\sigma'_{\mathrm{eff}}(\omega)=\sigma'(\omega)+\omega\varepsilon_0\varepsilon''_r(\omega). \tag{5}$$

Based on this concept, a critical frequency $f_C=\omega_C(2\pi)^{-1}$ follows with the definition of the loss factor $\tan\delta=\sigma_{\mathrm{eff}}(\omega_C)/[\omega_C\varepsilon_0\varepsilon_{r,\mathrm{eff}}(\omega_C)]=1$. Here the per cycle dissipated electrical energy due to charge transport is equal to the stored electrical energy due to high-frequency polarization processes. f_C is an important parameter in field applications: For $f<f_C$, the electrical conductivity σ_{eff} is the most effective parameter whereas is effective permittivity $\varepsilon_{r,\mathrm{eff}}$ for $f>f_C$. Especially in TDR applications, wave propagation is limited to the frequency range $f>f_C$ [*Wagner et al.*, 2007b].

2.1. Coupled Hydraulic-Mechanical-Electromagnetic Mixture Approach

[9] Porous mineral materials consist mainly of three phases: solid particles (various mineral phases), pore air, and a pore fluid. In principle, the fractions of the composite material phases vary both in space (due to composition and density of the material) and time (due to changes of water content, porosity, pore water chemistry, and temperature).

2.1.1. Mineral Matrix

[10] The electromagnetic properties of the solid particles are in general a second-order tensor (dyadic) with nine independent material parameters [see *Schoen*, 1996]. In the investigated temperature-pressure-frequency range, the

permittivity can be considered as frequency independent. Hence, relative effective permittivity of the solid matrix material $\varepsilon_{r,g}$ can be estimated from mineralogical composition of the solid phases [*Robinson*, 2004a, 2004b; *Robinson and Friedman*, 2003] assuming quasi-isotropy at the sample scale:

$$\varepsilon_{r,g} = \left(\sum_{k=1}^{N} w_k \frac{\rho_G}{\rho_{X,k}} \sqrt{\varepsilon_{g,k}} \right)^2, \tag{6}$$

with mass fraction w_k and $\sum_k w_k = 1$, X-ray density $\rho_{X,k}$ as well as relative effective real permittivity $\varepsilon_{g,k}$ of the appropriate kth phase obtained from the mineralogy. Moreover, several empirical equations were proposed relating relative effective permittivity of a material to its grain density ρ_g:

$$\varepsilon_{r,g} = A^{\rho_g} \tag{7}$$

such as the equations suggested by *Olhoeft* [1974] with $A = 1.93 \pm 0.17$ or *Campbell* [2002] with $A = 1.96$. A further empirical equation was suggested by *Dobson et al.* [1985]:

$$\varepsilon_{r,g} = (1.01 + 0.44 \cdot \rho_g)^2 - 0.062. \tag{8}$$

However, there is a lack of systematic broadband frequency and temperature-dependent high-resolution electromagnetic experimental investigations on appropriate solid monocrystalline/polycrystalline mineral phases. This issue needs to be addressed in further research activities.

2.1.2. Pore Fluid

[11] The pore fluid is an aqueous solution with a temperature-pressure-frequency–dependent relative complex permittivity according to the modified Debye model [*Kaatze*, 2007a; *Ellison*, 2007]:

$$\varepsilon_w^\star(\omega, T, p) - \varepsilon_\infty(T, p) = \frac{\Delta\varepsilon(T,p)}{1 + j\omega\tau_w(T,p)} - j\frac{\sigma_w(T,p)}{\varepsilon_0\omega}, \tag{9}$$

with direct current conductivity σ_w, high-frequency limit of permittivity ε_∞, relaxation strength $\Delta\varepsilon = \varepsilon_S + \varepsilon_\infty$ with static dielectric permittivity ε_S. The dielectric relaxation time τ_w depends on temperature T and pressure p according to Eyring's equation [*Buchner et al.*, 1999; *Logsdon and Laird*, 2004; *Kaatze*, 2007a]:

$$\tau_w(T,p) = \frac{h}{k_b T} \kappa \exp\left(\frac{\Delta G_w^\ddagger(T,p)}{RT} \right), \tag{10}$$

where h denotes Planck's constant, k_B Boltzmann's constant, $\kappa \approx 1$ the transmission coefficient, R gas constant, and $\Delta G_w^\ddagger(T,p) = \Delta H_w^\ddagger(T,p) - T\Delta S_w^\ddagger(T,p)$ free enthalpy or Gibbs energy of activation with activation enthalpy $\Delta H_w^\ddagger(T,p)$ and activation entropy $\Delta S_w^\ddagger(T,p)$.

[12] Furthermore, Gibbs energy of the interface fluid $\Delta G_d^\ddagger(T)$ is assumed to be a function of the distance from the particle surface (for quantitative approaches, see *Wagner and Scheuermann* [2009]). The matric potential Ψ_m of a porous material, introduced in soil science, is a measure of the bonding forces on water in the material and is related to the chemical potential of water $\Delta\mu_W = \mu_W^\circ - \mu_W = \Psi_m V_w$ with chemical potential at a reference state μ_W° and molar volume of water V_W [*Iwata et al.*, 1995; *Hilhorst et al.*, 2001]. Thus, *Hilhorst et al.* [2001, 2000; *Hilhorst*, 1998] suggested an approach for the relationship between Ψ_m and $\Delta G_d^\ddagger$:

$$\Psi_m(T) \cdot V_W = \Delta G_w^{\ddagger\circ}(T) - \Delta G_d^\ddagger(T), \tag{11}$$

with Gibbs energy of water at a reference state $\Delta G_w^{\ddagger\circ}(T)$ (10.4 kJ/mol at atmospheric conditions and $T = 293.15$ K). This relationship was used to calculate Gibbs energy of dielectric activation of interface water $\Delta G_d^\ddagger(T)$. Relative complex permittivity of free and interface water of a porous material, e.g., the Callovo-Oxfordian clay rock, in dependence of the volumetric water-content θ under atmospheric conditions then can be calculated [*Wagner et al.*, 2009]:

$$\Omega_a^\star(\theta, T) = \int_{\Psi_m(0)}^{\Psi_m(\theta)} \varepsilon_w^{\star a}(\Psi_m(\theta,T), T) \frac{\mathrm{d}\theta(\Psi_m)}{\mathrm{d}\Psi_m} \mathrm{d}\Psi_m. \tag{12}$$

In this form, a direct current conductivity contribution $\sigma_w(T)$ of the aqueous pore solution is implicitly included. The parameter $0 \leq a \leq 1$ is defined by the used mixture approach to obtain the relative effective complex permittivity of the material $\varepsilon_{r,\mathrm{eff}}^\star(\theta, T)$. The parameter a contains in principle structural information of the material including free and interface water and is strictly speaking a function of volumetric water content θ or water saturation S_w and porosity n [see *Wagner et al.*, 2011a].

2.1.3. Effective Electromagnetic Rock Properties

[13] *Hilhorst et al.* [2000] suggest the following theoretical mixture equation to model the effective permittivity of a porous material:

$$\varepsilon_{r,\mathrm{eff}}^\star(\theta, T) = \Omega_1^\star(\theta, T) + (1-n)\varepsilon_{r,G}(T) + (n-\theta). \tag{13}$$

For the incorporation of the bonding state of water as well as considering the pore water conductivity, the term $\Omega_H^\star(\theta, T) = \Omega_1^\star(\theta, T)$ then is given by [*Wagner and Scheuermann*, 2009]):

$$\Omega_H^\star(\theta, T) = \frac{\varepsilon_S(T) - \varepsilon_\infty}{3(2n-\theta)} \cdot \int_{\Psi(0)}^{\Psi(\theta)} \left[1 + j\frac{\omega h}{k_b T} e^{\frac{\Delta G_W(T)^\ddagger + |\Psi_m(\theta)| V}{RT}} \right]^{-1} \frac{\mathrm{d}\theta(\Psi)}{\mathrm{d}\Psi} \mathrm{d}\Psi + \theta \left(\varepsilon_\infty - j\frac{\sigma_{\mathrm{DC}}(T)}{3\omega\varepsilon_0(2n-\theta)} \right). \tag{14}$$

As an alternative approach, *Wagner et al.* [2011a] suggest the so-called advanced Lichtenecker and Rother Model:

$$\varepsilon_{r,\mathrm{eff}}^{\star a(\theta,n)}(\theta, T) = \Omega_{a(\theta,n)}^\star(\theta, T) + (1-n)\varepsilon_G(T)^{a(\theta,n)} + (n-\theta), \tag{15}$$

which is frequently used in CRIM (Complex Refractive Index Model) form with a constant structure parameter $a = 0.5$ [*Birchak et al.*, 1974; *Dobson et al.*, 1985; *Roth et al.*, 1990; *Mironov et al.*, 2004; *Wagner and Scheuermann*, 2009]. The term $\Omega_{\mathrm{CRIM}}^\star(\theta, T) = \Omega_{0.5}^\star(\theta, T)$ then has the following form:

$$\Omega_{\mathrm{CRIM}}^\star(\theta, T) = \int_{\Psi(0)}^{\Psi(\theta)} \varepsilon_w^{\star a}(\theta, T) \frac{\mathrm{d}\theta(\Psi)}{\mathrm{d}\Psi} \mathrm{d}\Psi. \tag{16}$$

Wagner et al. [2011a] further pointed out the dependence of apparent pore water conductivity σ_w in equation (9) on water saturation and porosity. A model for the effective conductivity of a water saturated rock $\sigma_{\mathrm{eff}}^\star$ is a modified Archie's law [*Patnode and Wyllie*, 1950; *Winsauer and McCardell*, 1953; *Schoen*, 1996]:

$$\sigma_{\mathrm{eff}}^\star = \frac{\sigma_w^\star}{F} + \sigma_s^\star, \tag{17}$$

with complex conductivity of the aqueous pore solution $\sigma_w^\star$, complex surface conductivity $\sigma_s^\star$, and formation factor $F = n^{-m}$ which can be related to porosity n with cementation exponent m. The theoretical model according to *Revil and Linde* [2006]

$$\sigma_{\text{eff}}^\star = \frac{\sigma_w^\star}{F} + \left(\frac{F-1}{F}\right)\sigma_s^\star \tag{18}$$

was used by *Jougnot et al.* [2010b] for the modeling of low-frequency electrical properties of the Callovo-Oxfordian clay rock. *Jougnot et al.* [2010b] suggest the following approach for modeling the complex pore water conductivity

$$\sigma_w^\star = \sigma_w + j\omega\varepsilon_0\varepsilon_w^\star, \tag{19}$$

with relative effective permittivity of water $\varepsilon_w^\star$ according to equation (9) as well as real direct current conductivity of the aqueous pore solution [*Jougnot et al.*, 2010b]:

$$\sigma_w = \sum_{k=1}^{N} \pm z_k e \beta_k \frac{C_k}{S_w}, \tag{20}$$

charge of an electron e, valency $\pm z_k$, ionic mobility in the solution β_k, and ionic concentrations in the pore space C_k of the kth ion species scaled with water saturation S_W. The model was applied under the assumption of a pure binary symmetric electrolyte such as NaCl and predicts an increase of σ_w with decreasing saturation, porosity, or volumetric water content. To account for this dependence in the mixture equation, the following empirical relationship with the normalized matric potential $\Psi_m' = \Psi_m/\Psi_m^{1\,\text{MPa}}$ suggested in *Wagner et al.* [2013] was used:

$$\sigma_w = A \cdot \Psi_m'^{\,B} + \sigma_{w,S}, \tag{21}$$

with empirical electrical conductivity coupling parameter $\log(A[S/m]) = -0.36 \pm 0.05$, shape factor $B = 0.572 \pm 0.007$, and a conductivity contribution at saturation $\sigma_{w,S}$.

3. Materials and Methods

3.1. Material Properties of the Clay Rock

[14] The ANDRA Underground Research Laboratory (URL) is located in the eastern part of the Paris Basin (≈300 km east of Paris) at 500 m depth in the Callovo-Oxfordian (COx) clay-rich sedimentary formation. The thickness of the COx formation is about 135 m at the URL location (–415 to –550 m). Its mineralogy is composed of clays minerals (mainly illite and interstratified illite/smectite, kaolinite, mica, and chlorite), tectosilicates (mainly quartz and feldspars), carbonates (mainly calcite and dolomite), and pyrite (<3%) (see Table 1) [*Gaucher et al.*, 2004]. The proportions of these components vary mainly depending on the depth of the sedimentary layer, leading to divide the layers into several geological units [*ANDRA*, 2012]. At the middle of the layer, where the URL is located, the clay content is maximal (≈50%–60%). Rock petrophysical and geochemical properties have been extensively studied on samples cored from several boreholes or in the URL. Several properties such as porosity, pore size distribution, mineral phase contents, ionic exchange capacity, sorption behavior, and transport properties have been measured. A complete review of COx properties can be found elsewhere [*Gaucher et al.*, 2004; *Sammartino et al.*, 2003]; however, the main characteristics are recalled hereafter. The porosity of the COx was determined using the water-content method in combination with nuclear magnetic resonance (NMR), porosity values mainly spread over 0.1 and 0.2, with a value of about 0.175 in the middle of the formation. Pores are mainly distributed between clay particles and within the interlayer space of swelling clay minerals (e.g., smectite). Pore diameter distribution characterized by mercury intrusion, NMR, and water adsorption range between nanometer and hundreds of nanometers [*Sammartino et al.*, 2003; *ANDRA*, 2012]. Meanwhile, the specific surface (measured by nitrogen adsorption) is relatively high with 27/36 m^2/g due to the high clay content. Transport properties are weakened due to these small pores. For instance, permeability is about 10^{-13} m^2. Clay-rich rocks are also characterized by their electrical properties. Clay platelets exhibit a net electric charge due to isomorphic ion substitutions. This results in a charge density of 0.8 e $(nm)^{-2}$ with the charge of an electron e and cationic exchange capacity ranges 14/15 mmol/100 g. The chemically equilibrated fluid contains about 0.1 *M*/L of ions. Therefore, the ionic transport leads to high direct current conductivity [see *Jougnot et al.*, 2010a]. In Table 1, the physicochemical data of the investigated samples are compiled.

3.2. Preparation of Rock Samples

[15] Once the main cores were taken from the formation of the underground laboratory, they were conserved in sealed bags to avoid contact with air. The first step of the shaping procedure consisted in overcoring the main core in order to obtain a rough specimen with a diameter larger than the finished specimen. Those "rough specimens" were held at different relative humidity in climatic chambers over saturated salt solutions as well as distilled water. After water-content stabilization was reached, checked by daily weighing, each rough specimen was shaped in order to obtain a perfect cylinder with the same dimensions of the sample holder (radii equal to 15 mm and height equal to 20 mm). *Wenk et al.* [2008] systematically studied the anisotropy of COx based on hard synchrotron X-ray measurements combined with Rietveld full diffraction image analysis. The results indicate a moderate anisotropy (axially symmetric about the normal to the bedding plane) of the phyllosilicates (illite and kaolinite) with a substantial proportion of randomly oriented crystallite. Furthermore, it was shown that the texture of calcite and quartz is essentially random. To avoid any systematic inference in our study due to the anisotropy of the clay rock, we used samples which were cored vertically to the stratigraphic sequence. Hence, the electrical field vector in the used TEM cell (transverse electric and magnetic field vectors to the propagation of the electromagnetic wave in the cell) is in parallel to the bedding plane and thus mainly parallel to the (001) plane of the phyllosilicates. Three specimens for six relative humidities were produced this way. Consequently, this preparation technique does not prevent the samples from pyrite oxidation. Nevertheless, pyrite represents less than 2% of the minerals and (see Table 2: Series 1/3/4 has 2% and Series 2 has 1%) its influence on the high-frequency electromagnetic material properties is assumed to be low [see *Comparon*, 2005] which was in addition confirmed by the analysis of the magnetic

Table 1. Physical, Chemical and Mineralogical Properties of the Investigated Callovo-Oxfordian Clay Rock for the Measurements Series 1,3,4/Series 2, Respectively[a]

Mineralogy, (wt %) Series 1,3,4/Series 2		Physicochemical Properties		Pore Water Chemistry	
Illite	22/16	Specific surface area	36/27 m^2/g	pH	7.2
Illite/smectite	20/19	Cation exchange capacity	14/15 mmol/100g	Eh (mV pr SHE)	–200
Kaolinite	5/0.5	Ionic Strength	0.08 mmol/L	Cl^- (mmol/L)	41
Chlorite	2/2.5	Particle density	2.67 g/cm^3	Na^+ (mmol/L)	43
Feldspars and quartz	22/31	Permittivty of solid particles	5.55	SO_4^{2-} (mmol/L)	15
Carbonates	26/30			HCO_3 (mmol/L)	2.1
Pyrite	2/1			Ca^{2+} (mmol/L)	8
Other	2/1			Mg^{2+} (mmol/L)	5
				K^+ (mmol/L)	1
				Sr^{2+}, Fe^{3+}, Si^{4+}	< 1

[a]For the samples of Series 1, all the cores were extracted from boreholes MCO1021 (depth 506 m), MCO1703 (503 m), and ORS1801 (496 m) of the geological unit UA2. For Series 2, core EST45405 from borehole DIR2004 (450 m) of geological unit USC2 was used as reference [*ANDRA*, 2012].

permeability obtained with the network analyzer measurements. Two samples were characterized whereas the third was conserved as a "check sample or witness/reference." Once the equilibrium was reached (for those small volumes, we have considered 3 weeks), a measurement of apparent density (geometrical measurement using a caliper) was made before drilling a hole to insert the inner conductor of the coaxial cell. Then each sample was placed in the cell and the electromagnetic characterization was performed. The only difficulty of this step was to manipulate the samples carefully. For the determination of the broadband electromagnetic properties, a close contact between inner and outer conductors of the coaxial transmission line was ensured to avoid additional low-frequency capacitive loss effects. Samples without a close contact were identified. These samples can only be used for the analysis of the dielectric material properties in the high-frequency range above 500 MHz. The last step of the procedure was the determination of the water content by mass, the porosity, and the degree of saturation. Water content was measured by loss of water using an oven held at 105°C. A second measurement was carried out at 150°C in nitrogen atmosphere for comparison with previous data. Due to clay-water interaction, 150°C dehydration is preferred to 105°C as some water remains between smectite platelets after drying at 105°C. Porosity was determined according to the dry density and a grain density equal to 2.7023 g/cm^3 [*Savoye et al.*, 2010] as well as the saturation degree (water content at 150°C) was accurately deduced from these parameters.

3.3. Parametrization of the Hydraulic and Structural Rock Properties

[16] The water sorption isotherm was parameterized based on soil physical concepts of the water retention characteristics. Therefore, in a first step relative humidity $\varphi = e/E$ (with vapor pressure of air e and saturation vapor pressure at sample temperature E) was converted to a water potential according to *Slatyer* [1967], *Dinulescu* [1979], and *Hilhorst et al.* [2001]:

$$\Psi_m(T) = \frac{RT}{V} \ln[\varphi(T)], \tag{22}$$

where R is the gas constant, T the absolute temperature of the sample, and V the partial molecular volume of water. In the next step, the water-retention characteristics are parameterized with a multimodal van Genuchten equation according to *Priesack and Durner* [2006]:

$$\frac{\theta - \theta_r}{\theta_S - \theta_r} = \sum_{i=1}^{N} w_i \left(\frac{1}{1 + [a_i|\Psi|]^{n_i}} \right)^{1-1/n_i}. \tag{23}$$

Herein, θ is volumetric water content, $|\Psi|$ matric potential, θ_r residual, and θ_S saturated volumetric water content; i counts for the number of the appropriate N subsystem with the weighting factors $0 \leq w_i \leq 1$ and van Genuchten parameters a_i and n_i. Changes of rock structure due to swelling with increasing humidity φ or decreasing water potential Ψ_m was parameterized with an empirical equation:

$$\frac{\rho'_D}{\rho_D} = \left(\frac{1}{1 + 10^{m(\theta - \theta_T)}} \right)^n, \tag{24}$$

with fictive dry density ρ'_D and dry density ρ_D at nearly zero saturation, volumetric transition water content θ_T, and empirical shape parameters m and n (see Figure 2); ρ'_D represents the appropriate dry density of the material at the actual water content. In Table 2, the results of the parametrization are compiled. This parameterized relationship then is used

Table 2. Parameters of Equation (23) With Appropriate Standard Deviation $\sigma_X = \sqrt{\mathrm{var}(\ldots)}$ As Well As Root-Mean-Square Error (RMSE) Estimates

	S1	σ_X	S2	σ_X	S3	σ_X	S4	σ_X	S5	σ_X
w [–]	0.79	0.02	0.84	0.03	0.771	0.006	0.84	0.02	0.75	0.02
a_1 [1/kPa]	3.2E-5	3E-6	3.7E-4	6E-5	2.06E-5	4E-7	2.2E-5	1.6E-6	4.7E-5	6E-5
a_2 [1/kPa]	0.049	0.008	5.0	0.8	0.024	0.004	0.044	0.007	0.047	0.007
n_1	1.768	0.038	1.32	0.04	1.991	0.019	1.958	0.041	1.737	0.040
n_2	1.99	0.13	1.96	0.16	2.19	0.15	2.09	0.15	2.17	0.12
RMSE [m^3/m^3]		0.076		0.096		0.037		0.052		0.073

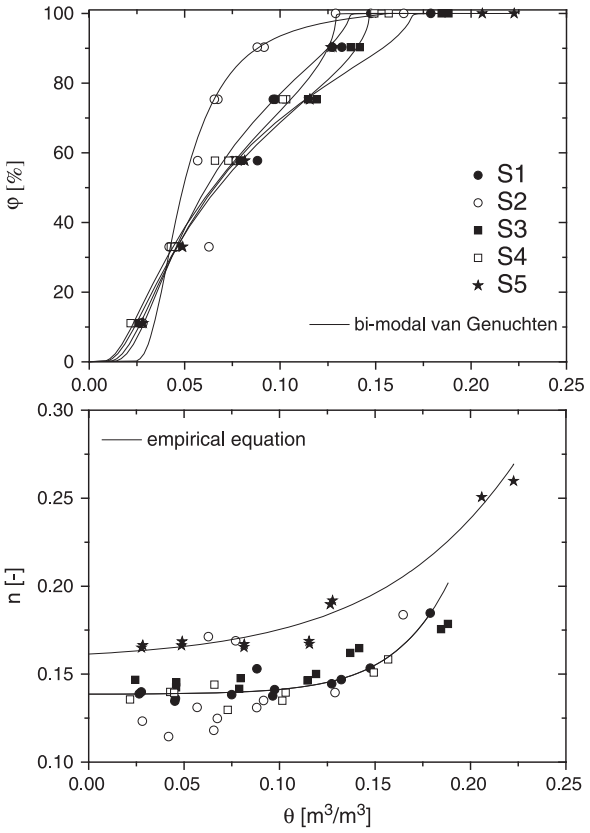

Figure 2. (top) Sorption isotherms of the samples parameterized with a bimodal van Genuchten relationships and (bottom) porosity n as a function of volumetric water content θ.

to determine the dependence of the porosity as a function of volumetric water content. The swelling/shrinkage processes affect pore size distribution and thus capillarity forces which in turn implicitly the dielectric properties. Hence, regardless of the stability of the permittivity-volumetric water-content relationship to changes in porosity at low volumetric water contents, porosity changes were considered in the modeling approach.

3.4. Dielectric Measurements

[17] The dielectric material properties were determined in the frequency range from 1 MHz to 10 GHz with network analyzer technique (Rhode and Schwarz ZVR, Agilent PNA, Anritsu VNA) in combination with two coaxial transmission line cells (Figure 3) [*Wagner et al.*, 2007b; *Lauer et al.*, 2010; *Ba and Sabouroux*, 2010; *Wagner et al.*, 2011a; *Lauer et al.*, 2012; *Wagner and Lauer*, 2012; *Bore et al.*, 2012]. The cells can be divided in three sections: two transition units and a specimen holder (Figure 3). The inner dimensions of the cells were determined in order to match the impedance of the source with 50 Ω yielding a condition of the ratio between inner diameter of the outer conductor b and outer diameter of the inner conductor a with $b/a = 2.302$. The technical details of the cells are compiled in Table 3.

[18] The cells were connected to a calibrated vector network analyzer (VNA) which sends a monochromatic electromagnetic wave and records the response of the sample by means of four complex scattering or S parameters (two transmission and two reflection factors, see *Baker-Jarvis et al.* [2004]). Prior to the S-parameter measurement, a full two-port (Short-Open-Load-Through) calibration procedure with mechanical standards was performed.

[19] In general, assuming propagation in TEM mode and non magnetic materials the relative effective complex permittivity $\varepsilon^{\star}_{r,\mathrm{eff}}$ of a sample in an ideal coaxial transmission line is related to its complex impedance $Z^{\star}_S$ or complex propagation factor $\gamma^{\star}_S$ as follows [*Nicolson and Ross*, 1970; *Baker-Jarvis et al.*, 2004 ; *Gorriti and Slob*, 2005a; *Wagner et al.*, 2010]:

$$\varepsilon^{\star}_{r,\mathrm{eff}} = \left(\frac{Z_0}{Z^{\star}_S}\right)^2, \tag{25}$$

$$\varepsilon^{\star}_{r,\mathrm{eff}} = \left(\frac{c_0\gamma^{\star}_S}{j\omega}\right)^2, \tag{26}$$

$$\varepsilon^{\star}_{r,\mathrm{eff}} = \frac{c_0 Z_0}{j\omega}\left(\frac{\gamma^{\star}_S}{Z^{\star}_S}\right). \tag{27}$$

Herein, Z_0 is the characteristic impedance of the empty transmission line, $c_0 = (\varepsilon_0\mu_0)^{-0.5}$ the velocity of light with ε_0. To obtain $Z^{\star}_S$ or $\gamma^{\star}_S$ from measured complex S-parameters S_{ij} several quasi-analytical approaches are available which lead to either equation (25), (26), or (27) as shown in *Gorriti and Slob* [2005b].

[20] *Nicolson and Ross* [1970] and *Weir* [1974] (NRW) introduced a quasi-analytical inversion procedures to obtain the frequency-dependent permittivity of low permittivity and low loss materials from measured S parameters. This approach was implemented in the software EpiMu by *Ba and Sabouroux* [2010] and used for the determination of the dielectric properties with the Anritsu VNA and IFSTTAR cell. *Baker-Jarvis* [1990] rigorously developed equations for the determination of the broadband electromagnetic material properties with coaxial transmission line cells from first principles and revisited the classical quasi-analytical algorithm according to NRW. In addition, new approaches were introduced including an iterative inversion technique which seems to be more robust and efficient in comparison to NRW called BJ and BJI. *Wagner et al.* [2010] and *Wagner et al.* [2011b] compare the quasi-analytical approaches based on 3-D finite element calculations in the frequency range between 1 MHz and 10 GHz in case of nondispersive low loss and strong dispersive standard materials with known frequency-dependent permittivity and showed the restriction in the applicability of the different techniques. Furthermore, in *Lauer et al.* [2012] and *Bohleber et al.* [2012], it was shown that the BJI approach is more stable than the quasi-analytical inversion.

[21] The first step in BJI is the application of NRW to the calibrated and preprocessed S parameters. The determined

Table 3. Geometrical Cell Parameters

Cell Name	IFSTTAR	MFPA
Connector type	APC-7	N-EIA 1 5/8”
Inner conductor —Outer diameter a (mm)	13.04	16.9
Outer conductor —Inner diameter b (mm)	30	38.8
—Outer diameter c (mm)	40	41.3
Length d (mm)	20	50
Sample volume V_C (cm^3)	11.47	47.90

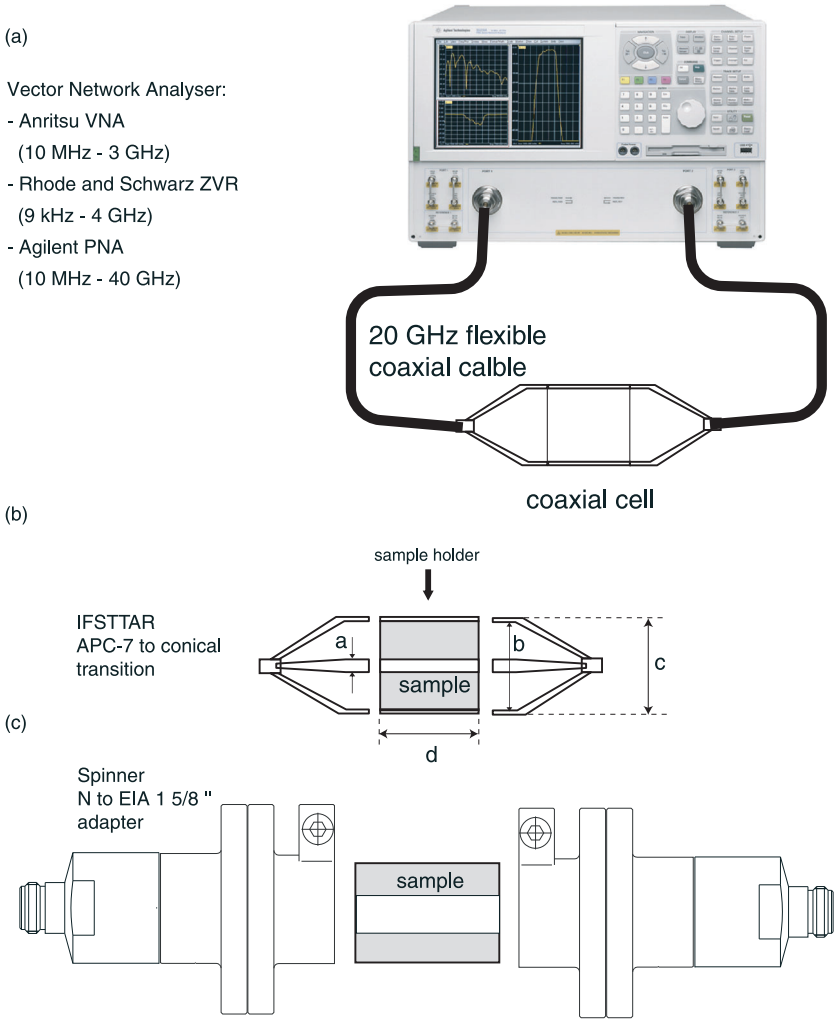

Figure 3. (a) Measurement setup to determine dielectric spectra with network analyzer technique in combination with coaxial transmission line cells. (b, c) Scheme of the used coaxial transmission line cells.

mean relative effective complex permittivity is used as starting guess for BJI. The permittivity $\varepsilon^{\star}_{r,\mathrm{eff}}$ is then obtained iteratively for every frequency by minimizing the difference D between measured and numerical calculated S parameters by means of a Levenberg-Marquardt algorithm [*Levenberg*, 1944; *Marquardt*, 1963] in Matlab based on the following equations:

$$f_1 = S_{11}S_{22} - S_{21}S_{12} - \frac{\Gamma^2 - \Xi^2}{1 - T^2\Gamma^2}, \tag{28}$$

$$f_2 = \frac{w_1(S_{21} + S_{12}) + (1 - w_1)(S_{11} + S_{22})}{2} - \frac{w_1\Xi(1 - \Gamma^2) + (1 - w_1)\Gamma(1 - T^2)}{1 - \Gamma^2 T^2} \tag{29}$$

and

$$D = \frac{w_2 f_1 + (1 - w_2) f_2}{2}. \tag{30}$$

with weighting factors $0 \leq w_i \leq 1$, ideal reflection factor Γ, and ideal transmission factor Ξ of a sample with length d in the coaxial transmission line defined as follows:

$$\Gamma = \frac{Z^{\star}_S - Z_0}{Z^{\star}_S + Z_0} \tag{31}$$

$$T = \exp(-\gamma^{\star}_S d); \tag{32}$$

with $Z^{\star}_S$ and $\gamma^{\star}_S$ provided by the relations (25) and (26). The Jacobian of the system is approximated using finite differences. To ensure stable results after the first 10 frequencies, the appropriate starting guess for the next frequency is calculated with the median of the previous 10 results. The BJI method is stable in the complete frequency range and can be applied to all S parameters separately or simultaneously with an appropriate weighting according to the stability of the experimental determined and preprocessed S parameters. The drawbacks of the BJI are the high sensitivity to uncertainties of the cell design or used calibration as well as the necessary starting guess to ensure stable convergence. Therefore, in this study, NRW technique and BJI were used in combination.

[22] A further approach to obtain the frequency-dependent permittivity is an inverse modeling technique based on the numerical calculation of the appropriate S parameters with a forward model (mostly TEM based) of the used coaxial transmission line cell in combination with a Debye-type relaxation function [*Oswald et al.*, 2006], a

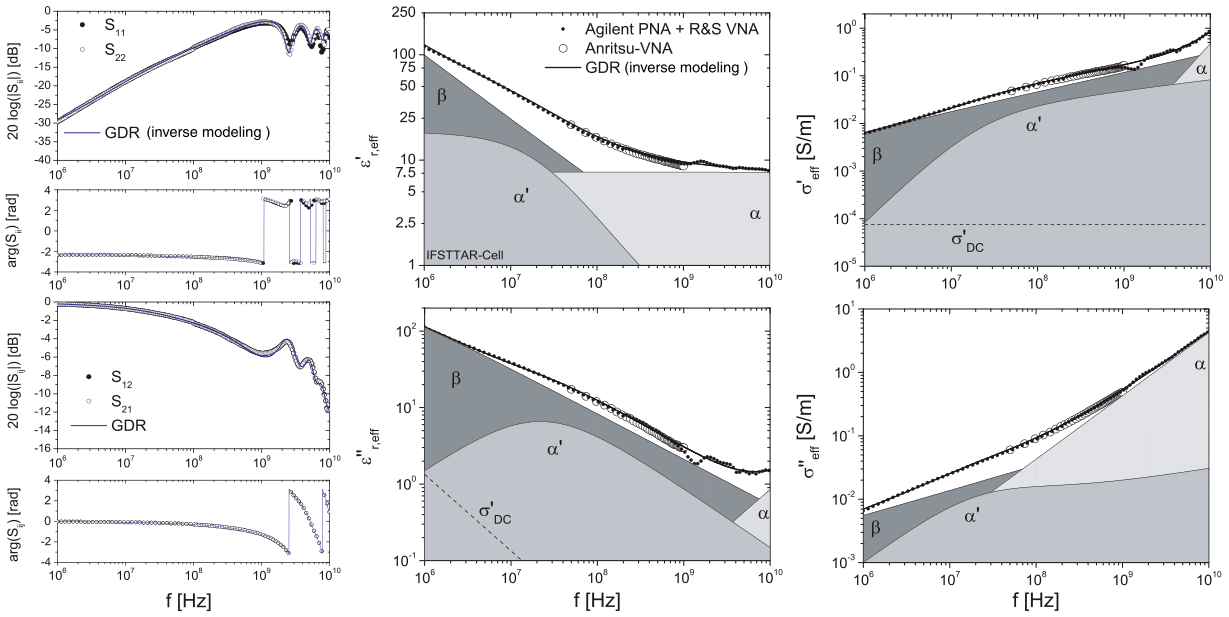

Figure 4. S parameter S_{ij}, complex effective relative permittivity $\varepsilon^{\star}_{r,\mathrm{eff}}$ and complex effective electrical conductivity $\sigma^{\star}_{\mathrm{eff}}$ as a function of frequency of a sample with volumetric water content $\theta = 0.066$ m^3/m^3, porosity $n = 0.14$, and saturation $S_W = 0.46$ as well as the results of inverse modeling with the SCEM-UA optimization (see text for the used terminology).

broadband transfer function (CCPM) [*Wagner et al.*, 2007c; 2011a] or a generalized dielectric relaxation model (GDR) [*Wagner et al.*, 2007c; 2011a]:

$$\varepsilon^{\star}_{r,\mathrm{eff}} - \varepsilon_{\infty} = \sum_{k=1}^{N} \frac{\Delta\varepsilon_k}{(j\omega\tau_k)^{a_k} + (j\omega\tau_k)^{b_k}} - j\frac{\sigma_{\mathrm{DC}}}{\omega\varepsilon_0} \tag{33}$$

with high-frequency limit of permittivity ε_{∞}, relaxation strength $\Delta\varepsilon_k$, relaxation time τ_k as well as stretching exponents $0 \leq a_k, b_k \leq 1$ of the kth process and apparent direct current electrical conductivity σ_{DC}. The technique can be used in equivalence to the BJI approach with measured S parameters separately or simultaneously. The advance of the approach is that Kramers-Kronig relations [*Kramers*, 1926; *Kronig*, 1926] are implicitly satisfied and thus unrealistic results due to the cell design or calibration will be avoided. Nevertheless, a substantial drawback is the lack of knowledge of the complexity of relaxation processes as well as electrode polarization effects and their consideration in the GDR formulation which in turn can lead to unstable results especially in case of available experimental data within a limited bandwidth. In principle, the relaxation models allow to link microscopic properties with the macroscopic material behavior and therefore offer the possibility of a generalization to a broad class of porous materials [*Wagner et al.*, 2007c; 2007a]. However, the development of robust generalized models requires careful systematic investigations on a wide range of unsaturated and saturated porous media under consideration of the multitude of influencing factors, such as the clay mineralogy, organic matter, pH and salinity of pore water, temperature, and porosity.

3.5. Analysis of Dielectric Spectra

[23] Equation (33) was fitted to the data set using a shuffled complex evolution Metropolis algorithm (SCEM-UA [*Vrugt et al.*, 2003]). This algorithm is an adaptive evolutionary Monte Carlo Markov chain method and combines the strengths of the Metropolis algorithm, controlled random search, competitive evolution, and complex shuffling to obtain an efficient estimate of the most optimal parameter set, and its underlying posterior distribution, within a single optimization run [*Heimovaara et al.*, 2004]. The algorithm is based on a Bayesian inference scheme. The needed prior information is a lower and upper bound for each of the relaxation parameters ξ. Assuming this noninformative prior the posterior density $p(\xi|\mathbf{y}, \gamma)$ for ξ conditioned with the measurement $\mathbf{y}$ is given by [*Vrugt et al.*, 2003]:

$$p(\xi|\mathbf{y}, \gamma) \propto \left[\sum_{k=1}^{N}\left(\frac{y_k - \hat{y}_k}{\delta}\right)\right]^{\frac{-N(1+\gamma)}{2}}. \tag{34}$$

Herein, y_k is the kth of m measurements at each frequency for a given temperature and $\hat{y}_k$ is the corresponding model prediction; δ represents the error of the measurements expressed as a standard deviation. The parameter γ specifies the error model of the residuals. In this study, we assume a normal distribution with $\gamma = 0$. To characterize the relaxation behavior, three processes are assumed to act in the investigated frequency-temperature-pressure range: one primary α process (main water relaxation) and two secondary (α', β) processes due to clay-water-ion interactions (bound water relaxation, counter ion relaxation, and Maxwell-Wagner effects respectively, see *Wagner et al.* [2007b]). In the presented high-frequency approach, the dynamic transition linked with the structural α transition is the main water relaxation process which can be identified with a high accuracy. However, this process is not the slowest dielectric relaxation process of the heterogeneous multiphase porous material. Due to the impossibility to see the slowest relaxation process, we label the water process with α and count

with decreasing frequency. Furthermore, an apparent direct current conductivity contribution is considered.

4. Results and Discussion

[24] The dielectric relaxation behavior of a clay-rock sample of Series 4 (S4) at an intermediate saturation is shown in Figure 4. In Table 4, the relaxation parameters for the analyzed data sets are summarized. The results clearly indicate stable relaxation parameters with a moderate uncertainty for the two high frequency relaxation processes α, α' (see Figure 5). However, the low-frequency relaxation parameters of the β process show a high uncertainty. Hence, the frequency range has to be extended to

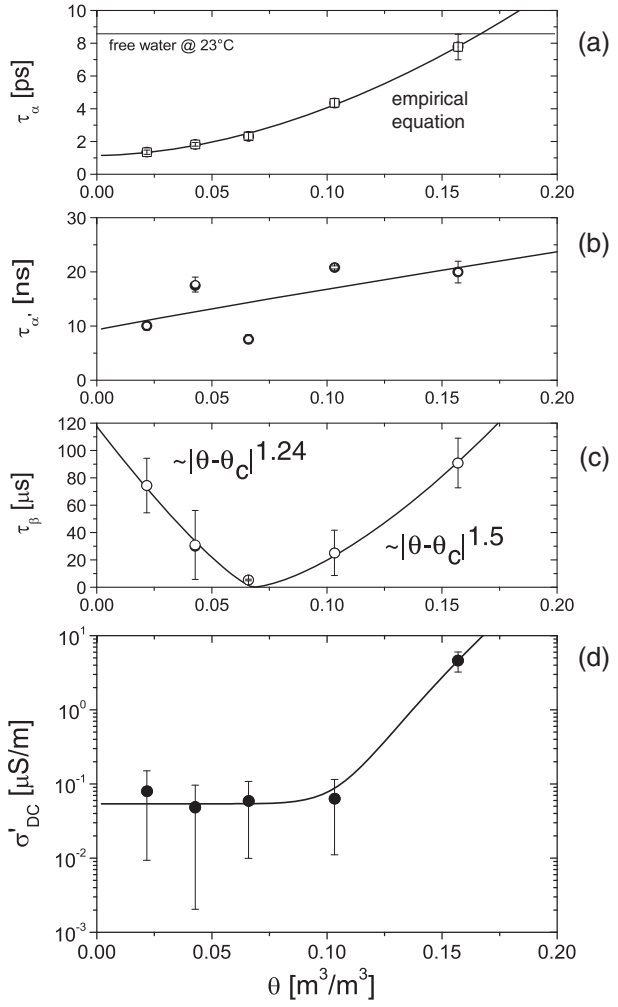

Figure 5. Results of the parametrization of the relaxation behavior obtained with the SCEM-UA optimization based on the broadband relaxation model from the measurements with the IFSTTAR-cell (see section 3.5). (a–c) Appropriate relaxation time τ_i for α, α', and β process as well as (d) apparent direct current conductivity σ'_{DC} as a function of volumetric water content θ. The lines in Figures 5a, 5b, and 5d were calculated based on an empirical relationship between volumetric water content θ and appropriate property y with $y = a_1 + a_2\theta^{a_3}$.

Table 4. Results of the Inverse Modeling With Equation (33)[a]

θ (m^3/m^3)	n	S_w	ε_S	ε_∞	$\Delta\varepsilon_\alpha$	τ_α (ps)	$\Delta\varepsilon_{\alpha'}$	$\tau_{\alpha'}$ (ns)	$1-a_{\alpha'}$	$\Delta\varepsilon_\beta$	τ_β (μs)	$1-a_\beta$	σ (μS/m)
0.022	0.136	0.160	6.21	1.50 (0.4)	4.72 (0.4)	1.35 (0.13)	13.2 (0.7)	10.1 (0.8)	0.383 (0.004)	789 (311)	74.4 (19.9)	0.27 (0.04)	0.08 (0.07)
0.043	0.140	0.306	6.81	1.48 (0.3)	5.33 (0.3)	1.83 (0.11)	36.2 (2.4)	17.5 (1.3)	0.353 (0.004)	1069 (376)	30.0 (25)	0.33 (0.02)	0.05 (0.05)
0.066	0.144	0.458	7.71	1.73 (0.5)	5.98 (0.5)	2.33 (0.23)	20.1 (3.0)	7.6 (0.8)	0.234 (0.027)	1312 (89)	5.3 (0.6)	0.40 (0.01)	0.05 (0.05)
0.103	0.139	0.740	9.29	4.11 (0.3)	5.18 (0.3)	4.35 (0.28)	129.9(1.6)	20.8 (0.3)	0.276 (0.001)	1148 (210)	25.1 (16.5)	0.27 (0.02)	0.06 (0.05)
0.157	0.158	0.991	11.06	8.19(1.6)	2.87 (0.5)	7.77 (0.78)	172.1(34.4)	20.0 (1.9)	0.31 (0.06)	24115 (1220)	90.9 (18.2)	0.005 (0.001)	4.6n (1.4)

[a] As well as calculated static permittivity of the free water term $\varepsilon_{S,FW} = \Delta\varepsilon_{FW} + \varepsilon_\infty$ obtained by means of 10,000 samples generated after convergence to a posterior distribution (mean value and in brackets appropriate standard deviation).

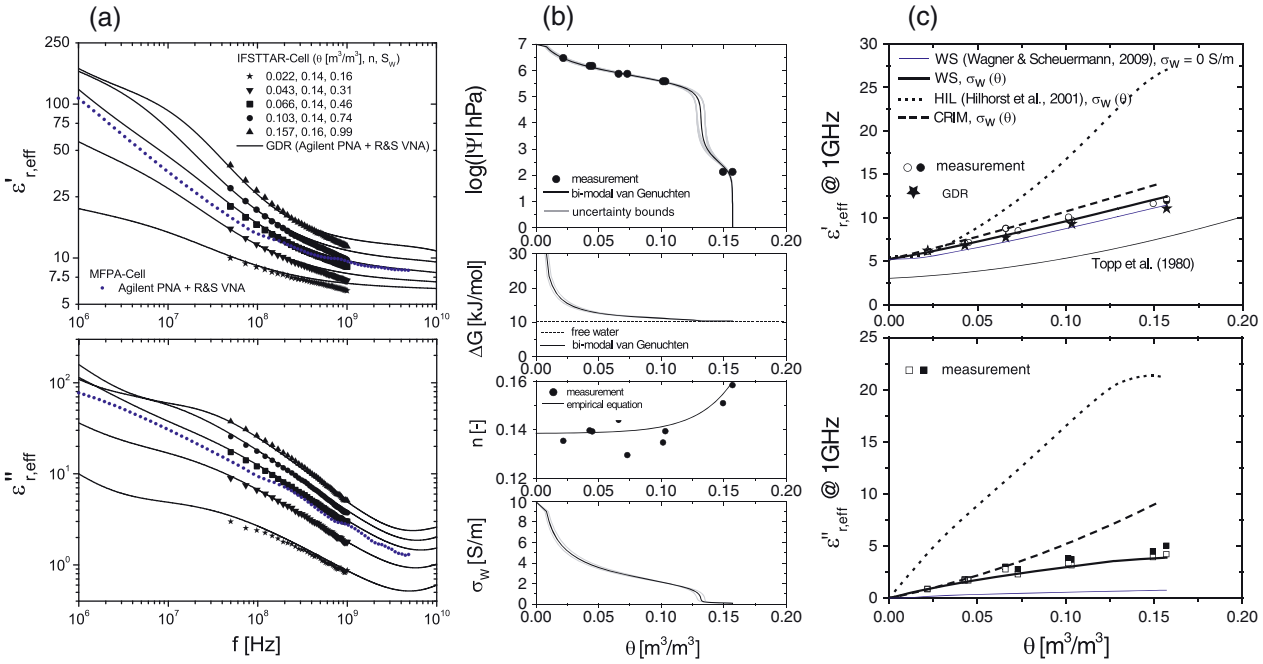

Figure 6. (a) Dielectric spectra of the clay-rock from series 4 (S4) as a function of frequency at different states. Indicated are the results obtained with the IFTTAR cell measured with the Anritsu VNA as well as R&S and Agilent PNA. Furthermore, the results obtained with the MFPA cell were additionally indicated. (b) From top to bottom, water potential Ψ_m, free enthalpy or Gibbs energy of activation $\Delta G_d^{\ddagger}$, porosity n, and apparent pore water conductivity σ_w in equation (9). (c) Application of the coupled hydraulic-mechanic-dielectric mixture approach at a frequency of 1 GHz.

lower frequencies in further studies. Moreover, to fully characterize the underlying kinetics of the relaxation behavior, the temperature dependence has to be investigated. Furthermore, the estimated apparent direct current conductivity contribution σ'_{DC} represents an upper boundary due to the certainty low absolute values with appropriate uncertainty (see Figures 4 and 5). The systematic increase of the static permittivity as well as relaxation time of the α process indicates the presence of pore water (see schematic in Figure 1). The obtained relaxation time is slightly higher than free water relaxation with 8.7 ps at 23°C [*Kaatze*, 2007b] associated with water hydrogen network fluctuations. However, due to the strong α' process with relaxation times between 7.6 and 20.8 ns, the water signal is overlapped in the frequency range of microwave applications (Figure 5). Therefore, in case of practical application, apparent permittivity obtained with HF-EM techniques contains not only the water-content contribution but also effects due to water-mineral interaction processes. These processes are a superposition of interface (adsorbed or hydrated) water with relaxation times in the MHz range [*Logsdon and Laird*, 2004; *Bergman and Swenson*, 2000] as well as relaxation effects referred to as adsorption/desorption rates of counter ions in clay interlayers with relaxation times in the range between 2 and 8 ns [*Rotenberg et al.*, 2005]. The low-frequency range is dominated by a broad β-relaxation process attributed to a distribution of Maxwell-Wagner effects superimposed with low-frequency counter ion relaxation effects with a broad distribution of relaxation times > 1 μs [*Leroy and Revil*, 2009; *Revil*, 2013]. In general, in a partly saturated porous material, a broad distribution of relaxation times is expected to appear which depends on the ion speciation, concentration, pore water chemistry and spatial scales which can be explored by an ion in the complex shaped pore space which is moreover constraint by grain boundaries, inter-granular porosity and air-water interface [*Rotenberg et al.*, 2005; *Leroy et al.*, 2008; 2012, *Leroy and Revil*, 2009; *Revil*, 2013]. Therefore, with high-frequency electromagnetic measurements, it is difficult to clearly separate the different counter ion relaxation effects as well as MW processes. Consequently, it is recommended to combine low- and high-frequency techniques on the same material analyzed under defined boundary conditions (fluid pressure, temperature, stress-strain state). Apparent direct current contribution σ_{DC} is low in comparison to the relaxation processes and an inference with the low-frequency relaxation processes as well as electrode polarization effects is strongly suppressed.

[25] In Figure 6 complex effective permittivity $\varepsilon''_{r,eff}$ determined with the IFSTTAR cell with the three VNAs as a function of frequency for the samples from Series 4 (S2) at different states is represented. In comparison, the result measured with the MFPA cell was included which indicates the broadband capabilities of the MFPA cell design. Due to the slight differences in the samples, the material properties are different at the same temperature and relative humidity (cf. Figure 2) so that the results are not absolutely identical. The spectra show the systematic relationship between water content and permittivity in the microwave range above 1 GHz. This relationship for the α process is also given in Figure 7 in

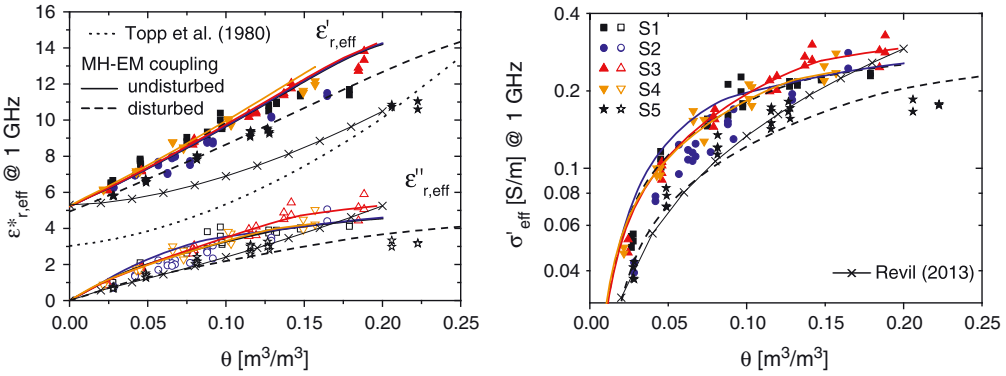

Figure 7. (left) Measured complex effective relative permittivity $\varepsilon^{\star}_{r,\mathrm{eff}} = \varepsilon'_{r,\mathrm{eff}} - j\varepsilon''_{r,\mathrm{eff}}$ and (right) real part of complex electrical conductivity σ'_{eff} at a measurement frequency of 1 GHz in comparison with the frequently used empirical equation according to *Topp et al.* [1980], a recent broadband model suggested by *Revil* [2013], and the results of the proposed HM-EM approach.

comparison to measured and modeled effective permittivity with different methods at a frequency of 1 GHz.

[26] The hydraulic-mechanical-electromagnetic mixture approach was applied using the two mixture equations (13) and (15) with and without consideration of the binding state of water according to the applied relative humidity as well the dependence of the pore water conductivity on water content. Furthermore, the empirical relationship between volumetric water content and effective permittivity according to *Topp et al.* [1980] frequently used in geophysical applications was applied to the data set. A novel broadband model was recently suggested by *Revil* [2013] based on a linear volumetric homogenization approach for the constitutive electromagnetic material equations combined with first and second Archie's laws. In the high-frequency range assuming that fist and second Archie exponents are equal $m \approx n$, this gives

$$\sigma'_{\mathrm{eff}} \approx \theta^m \sigma'_w + \theta^{m-1}\sigma'_s \tag{35}$$

$$\varepsilon'_{r,\mathrm{eff}} \approx \theta^m \varepsilon'_w + \varepsilon_{r,g} \tag{36}$$

with the effective conductivity σ'_{eff}, real electrical conductivity of the pore fluid σ'_w, real surface conductivity contribution σ_s, and real permittivity of water ε'_w. The suggested model parameters were determined based on a 1.3 GHz data set measured by *Comparon* [2005] on a bentonite-kaolinite mixture with $m = 1.7 \pm 0.1$ and $\sigma_s = 0.44 \pm 0.1$. For the permittivity of the solid phase $\varepsilon_{\mathrm{r,g}}$ the estimate in this study is used (see Table 1).

[27] The results clearly show that the empirical equation can not be used in case of this clay rock due to the inability to consider the real rock structure, i.e., porosity. At low water contents < 5 vol % both mixture equations predict the real part of complex permittivity in reasonable agreement with the experimental results. With increasing water content, the approach according to the mixture equation of *Hilhorst et al.* [2000] overestimates $\varepsilon^{\star}_{r,\mathrm{eff}}$ due to the structure of the mixture model (see discussion in *Wagner and Scheuermann* [2009] and *Wagner et al.* [2011b]). The modified hydraulic-mechanical-electromagnetic mixture approach according to *Wagner et al.* [2011b] gives reasonable results. The influence of interface (adsorbed or hydrated) water on the real part of the complex effective permittivity at a typical frequency of 1 GHz is much lower than expected which was already recognized in *Wagner et al.* [2011b]. In the imaginary part, the influence of the interface water effects is much stronger. The comparison between the mixture equation without consideration of interface water but incorporation of the dependence of the apparent conductivity of pore water as a function of water content clearly shows that the interface water has to be considered. This becomes also clear from the imaginary part of $\varepsilon^{\star}_{r,\mathrm{eff}}$. The interface water contribution in the imaginary part is low in comparison to the conductivity effect. Therefore, the suggested coupling between conductivity and matric potential was used instead of equation (20) to implicitly consider all conductivity contributions. The model according to *Revil* [2013] with the used parameters clearly shows the potential of the proposed approach to predict the complex permittivity or conductivity in the high frequency range in alternative to classical mixture equations. However, appropriate Archie exponents as well as the surface conductivity contribution have to be coupled with hydraulic and mechanical properties in a next step to consider the complete relaxation dynamics.

[28] However, the comparison of the predicted bound water relaxation with the obtained relaxation processes based on the broadband generalized fractional relaxation model (GDR) indicates that the interface water relaxation is superimposed by additional processes. In Figure 8, the imaginary part $\varepsilon''_{r,\mathrm{eff}}$ of the complex effective permittivity is plotted as a function of free enthalpy of activation given by

$$\Delta G_d^{\ddagger} = RT \ln\left(\frac{\hbar}{k_B T f}\right) \tag{37}$$

with gas constant R, absolute temperature T, Dirac constant $\hbar = h_P(2\pi)^{-1}$, Planck constant h, Boltzmann constant k_B, and frequency f. With the proposed model, the water relaxation processes in the aqueous pore solution due to hydrogen network fluctuation as well as interface water relaxation with Gibbs energies of activation between 10 and 20 kJ/mol were considered. Hence, $\Delta G_d^{\ddagger}$ of interface water is well below that of ice with 60 kJ/mol. The observed decrease below 10 kJ/mol with decreasing saturation is in contrast to the expected increase of $\Delta G_d^{\ddagger}$ of interface water [*Wagner and Scheuermann*, 2009]. Determined Gibbs energy of the observed low-frequency β process is in

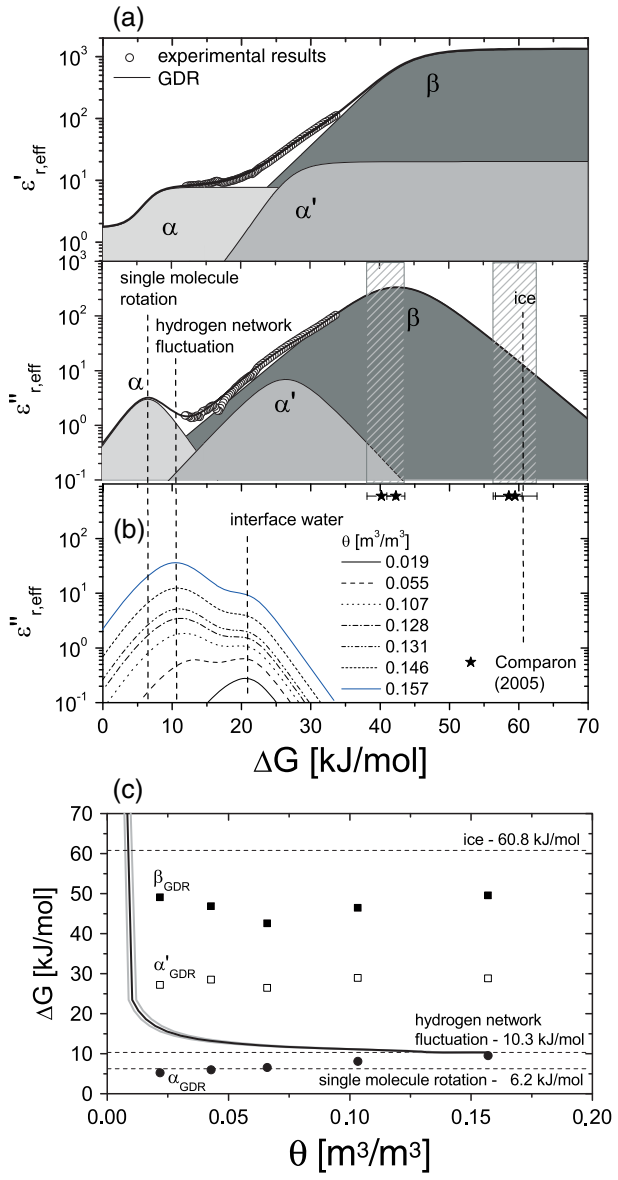

Figure 8. (a) Real $\varepsilon'_{r,\mathrm{eff}}$ and imaginary part $\varepsilon''_{r,\mathrm{eff}}$ of the complex relative effective permittivity obtained with the broadband generalized fractional relaxation model (GDR) and subtracted apparent direct current conductivity σ'_{DC} contribution. (b) Appropriate imaginary part $\varepsilon''_{r,\mathrm{eff}}$ of the modeled effective permittivity based on the hydraulic-mechanical-electromagnetic mixture approach for sample C4 (see Figure 4) as a function of free enthalpy of activation calculated based on equation (10) with $\tau = (2\pi f)^{-1}$. (c) Free enthalpy of activation or Gibbs energy $\Delta G_d^{\ddagger}$ according to equation (11) as a function of volumetric water content θ.

close agreement with the provided results of the study by *Comparon* [2005] regardless of the different measurement and analysis approach. However, due to the restricted frequency range in the presented study, the proposed relaxation process with Gibbs energy close to ice was not able to predict.

[29] A comparison of Gibbs energy of the high-frequency water relaxation process with 6.2 kJ/mol, associated with single molecule rotation [*Buchner et al.*, 1999; *Kaatze*, 2007b], coincidence with $\Delta G_d^{\ddagger}$ of the experimental determined high frequency α process (see Figure 8). With increase in water content or saturation the process associated with hydrogen network fluctuation becomes dominant.

5. Conclusion

[30] The dielectric relaxation behavior of Callovo-Oxfordian clay rock from the formation of the planed underground repository in Bure, France (Meuse district, eastern Paris Basin, France), was studied in the frequency range from at least 1 MHz to 10 GHz at atmospheric conditions with network analyzer technique in combination with coaxial transmission line cells. For this purpose, undisturbed and disturbed clay-rock samples were conditioned at defined relative humidity between 10% and nearly 100% to achieve a water saturation range from at least 0.16 to nearly saturation. The relaxation behavior was quantified based on a broadband generalized fractional relaxation model under consideration of an apparent direct current contribution assuming three relaxation processes: a high-frequency water process with relaxation times τ_α between 1.4 and 7.8 ps and two interface processes which are related to interactions between the aqueous pore solution and mineral particles such as adsorbed and hydrated water relaxation superposed with counter ion relaxation processes with $\tau_{\alpha'}$ between 7.6 an 20.8 ns, Maxwell-Wagner effects with $\tau_\beta > 1$ μs and low-frequency counter ion relaxation effects. The frequency-dependent HF-EM properties were further modeled based on a novel hydraulic-mechanical-electromagnetic coupling approach developed for soils under consideration of the water sorption isotherm as well as structural changes due to swelling effects. The proposed model allows a quantification of free and interface water relaxation processes as well as a coupling to the high-frequency electrical conductivity contribution in the aqueous pore solution. Hence, the approach enables the modeling of the dependence of the complex permittivity as a function of water content or water saturation and porosity in the frequency range of TDR applications around 1 GHz in reasonable agreement with experimental results. The comparison of the dielectric relaxation behavior of interface water predicted with the proposed mixture approach with the results from the broadband analysis with GDR indicates a more complicated behavior of the electromagnetic wave interaction with water in the clay rock. In addition to the free and interface water relaxation processes due to the fluctuation of the hydrogen bounded network, a high-frequency mechanism is suggested with Gibbs energy of activation close to single water molecule relaxation. However, the results show the potential of HF-EM techniques for quantitative monitoring of the hydraulic state in underground repositories in clay formations. Based on the findings in the presented study, it is suggested to develop a measurement setup which allows the analysis of core samples under defined mechanical and hydraulic conditions by means of a combination of low and high frequency measurement techniques (from mHz to microwave). An additional issue which has to be addressed in further research activities is the numerical 3-D analysis of the effect of anisotropy of

the clay rock on the high-frequency electromagnetic properties in equivalence to the studies on transport properties by *Robinet et al.* [2012].

[31] **Acknowledgments.** The authors would like to thank Claude Gatabin from the CEA Saclay. He was in charge of all the samples preparation and the characterization. Moreover, the authors gratefully acknowledge the German Research Foundation (DFG) for support of the project WA 2112/2. Furthermore, the authors would like to acknowledge André Revil for his valuable comments and suggestions.

References

ANDRA, (2012), Référentiel du site meuse/haute-marne, tome 1-le site de meuse/haute marne: Histoire géologique et état actuel., *Tech. rep.*, ANDRA, Paris.

Arcone, S., S. Grant, G. Boitnott, and B. Bostick (2008), Complex permittivity and clay mineralogy of grain-size fractions in a wet silt soil, *Geophysics*, *73*(3), J1–J13, doi:10.1190/1.2890776.

Ba, D., and P. Sabouroux (2010), Epsimu, a toolkit for permittivity and permeability measurement in microwave domain at real time of all materials: Applications to solid and semisolid materials, *Microwave Opt. Technol. Lett.*, *52*(12), 2643–2648.

Baker-Jarvis, J. (1990), Transmission/reflection and short circuit line permittivity measurements, *Tech. Rep.*, NIST, U.S. Department of Commerce.

Baker-Jarvis, J., M. D. Janezic, B. Riddle, R. T. Johnk, P. Kabos, C. L. Holloway, R. G. Geyer, and C. A. Grosvenor, (2004), Measuring the permittivity and permeability of lossy materials: Solids, liquids, metals, building materials, and negative-index materials, *Tech. Rep. 1536*, National Institute of Standards and Technology-NIST, U.S. Department of Commerce.

Behari, J. (2005), *Microwave Dielectric Behaviour of Wet Soils*, Springer, New Delhi, India.

Bergman, R., and J. Swenson (2000), Dynamics of supercooled water in confined geometry, *Nature*, *403*(6767), 283–286.

Birchak, J., C. Gardner, J. Hipp, and J. Victor (1974), High dielectric constant microwave probes for sensing soil moisture, *Proc. IEEE*, *62*(1), 93–98.

Bohleber, P., N. Wagner, and O. Eisen (2012), Permittivity of ice at radio frequencies: Part I: Coaxial transmission line cell, *Cold Reg. Sci. Technol.*, *82*, 56–67.

Bore, T., D. Placko, D. Coelho, S. Delepine-Lesoille, C. Gatabin, P. Sabouroux, G. Six, and F. Taillade (2012), Design and evaluation of two coaxial transmission lines to characterize electromagnetism properties of hard clays (non crushed) and concrete, in *Proc. of the Advanced Electromagnetics Symposium, AES 2012*, edited by S. Zoudhi and X. Begaut, pp. 546–555, Telecom Paristech, Paris, France.

Börner, F. (2006), Groundwater Geophysics, A Tool for Hydrogeology, in *chap. Complex Conductivity Measurements*, edited by R. Kirsch, pp. 119–153, Springer, Berlin Heidelberg, New York.

Buchner, R., J. Barthel, and J. Stauber (1999), The dielectric relaxation of water between 0°C and 35°C, *Chem. Phys. Lett.*, *306*(1–2), 57–63.

Campbell, B. (2002), *Radar Remote Sensing of Planetary Surfaces*, Cambridge University Press, Cambridge, U.K.

Chen, Y., and D. Or (2006), Effects of Maxwell-Wagner polarization on soil complex dielectric permittivity under variable temperature and electrical conductivity, *Water Resour. Res.*, *42*, W06424, doi:10.1029/2005WR004590.

Comparon, L. (2005), Etude experimentale des proprietes electriques et dielectriques des materiaux argileux consolides, PhD thesis, Institut de physique du globe de Paris-IPGP.

Delay, J., A. Lesavre, and Y. Wileveau (2008), The French Underground Research Laboratory in Bure as a precursor for deep geological repositories, *Rev. Eng. Geol.*, *19*, 97–111.

Dinulescu, H. (1979), Thermodynamic state functions of the soil water system, *Heat Mass Transfer*, *12*(3), 243–259.

Dobson, M. C., F. T. Ulaby, M. T. Hallikainen, and M. A. El-Rayes (1985), Microwave dielectric behavior of wet soil—Part II: Dielectric mixing models, *IEEE Trans. Geosci. Remote Sens.*, *GE-23*(1), 35–46.

Ellison, W. J. (2007), Permittivity of pure water, at standard atmospheric pressure, over the frequency range 0–25 tHz and the temperature range 0–100°C, *J. Phys. Chem. Ref. Data*, *36*(1), 1–18.

Folgero, K. (1998), Broadband dielectric spectroscopy of low-permittivity fluids using one measurement cell, *IEEE Trans. Instrum. Meas.*, *47*(4), 881–885.

Gaucher, E., et al. (2004), ANDRA underground research laboratory: Interpretation of the mineralogical and geochemical data acquired in the Callovian–Oxfordian formation by investigative drilling, *Phys. Chem. Earth*, *29*(1), 55–77.

Gorriti, A., and E. Slob (2005a), Comparison of the different reconstruction techniques of permittivity from S-parameters, *IEEE Trans. Geosci. Remote Sens.*, *43*(9), 2051–2057.

Gorriti, A., and E. Slob (2005b), Synthesis of all known analytical permittivity reconstruction techniques of nonmagnetic materials from reflection and transmission measurements, *IEEE Trans. Geosci. Remote Sens.*, *2*(4), 433–436.

Hallikainen, M. T., F. T. Ulaby, M. C. Dobson, M. A. El-Rayes, and L.-K. Wu (1985), Microwave dielectric behavior of wet soil—Part I: Empirical models and experimental observations, *IEEE Trans. Geosci. Remote Sens.*, *GE-23*(1), 25–34.

Heimovaara, T. J., J. A. Huisman, J. A. Vrugt, and W. Bouten (2004), Obtaining the spatial distribution of water content along a TDR probe using the SCEM-UA Bayesian inverse modeling scheme, *Vadose Zone J.*, *3*, 1128–1145.

Heimovaara, T., W. Bouten, and J. Verstraten (1994), Frequency domain analysis of time domain reflectometry waveforms, 2. A four-component complex dielectric mixing model for soils, *Water Resour. Res.*, *30*(2), 201–209.

Hilhorst, M. (1998), Dielectric characterisation of soil, PhD thesis, Wageningen Agricultural University, The Netherlands.

Hilhorst, M., C. Dirksen, F. Kampers, and R. Feddes (2000), New dielectric mixture equation for porous materials based on depolarization factors, *Soil Sci. Soc. Am. J.*, *64*(5), 1581–1587.

Hilhorst, M., C. Dirksen, F. Kampers, and R. Feddes (2001), Dielectric relaxation of bound water versus soil matric pressure, *Soil Sci. Soc. Am. J.*, *65*(2), 311–314.

Hoekstra, P., and A. Delaney (1974), Dielectric properties of soils at UHF and microwave frequencies, *J. Geophys. Res.*, *79*(11), 1699–1708.

Ishida, T., T. Makino, and C. Wang (2000), Dielectric-relaxation spectroscopy of kaolinite, montmorillonite, allophane, and imogolite under moist conditions, *Clays Clay Miner.*, *48*(1), 75–84.

Ishida, T., M. Kawase, K. Yagi, J. Yamakawa, and K. Fukada (2003), Effects of the counterion on dielectric spectroscopy of a montmorillonite suspension over the frequency range 10e5-10e10 Hz, *J. Colloid Interface Sci.*, *268*(1), 121–126.

Iwata, S., et al. (1995), *Soil-Water Interactions: Mechanisms and Applications,* 2nd ed., Marcel Dekker, Inc., New York.

Jonscher, A. K. (1977), The universal dielectric response, *Nature*, *267*(5613), 673–679.

Jonscher, A. K. (1983), *Dielectric Relaxation in Solids*, Chelsea Dielectrics Press, London.

Jougnot, D., A. Revil, N. Lu, and A. Wayllace (2010a), Transport properties of the Callovo-Oxfordian clay rock under partially saturated conditions, *Water Resour. Res.*, *46*, W08514, doi:10.1029/2009WR008552.

Jougnot, D., A. Ghorbani, A. Revil, P. Leroy, and P. Cosenza (2010b), Spectral induced polarization of partially saturated clay-rocks: A mechanistic approach, *Geophys. J. Int.*, *180*(1), 210–224, doi:10.1111/j.1365-246X.2009.04426.x.

Kaatze, U. (2007a), Non-conducting and conducting reference liquids for the calibration of dielectric measurement systems, in *Proc. of the 7th International Conference on Electromagnetic Wave Interaction with Water and Moist Substances*, edited by S. Okamura, pp. 3–11, ISEMA, Hamamatsu, Japan.

Kaatze, U. (2007b), Reference liquids for the calibration of dielectric sensors and measurement instruments, *Meas. Sci. Technol.*, *18*(4), 967–976.

Kaatze, U., and Y. Feldman (2006), Broadband dielectric spectrometry of liquids and biosystems, *Meas. Sci. Technol.*, *17*(2), R17–R35.

Katsube, T., and L. Collet (1974), The physics and chemistry of minerals and rocks, in *Electromagnetic Propagation Characteristics of Rocks*, edited by R. G. J. Strens, pp. 279–295, John Wiley & Sons, London, U.K.

Kelleners, T. J., D. A. Robinson, P. J. Shouse, J. E. Ayars, and T. H. Skaggs (2005), Frequency dependence of the complex permittivity and its impact on dielectric sensor calibration in soils, *Soil Sci. Soc. Am. J.*, *69*(1), 67–76.

Kramers, H. (1926), The quantum theory of dispersion, *Nature*, *117*, 775.

Kremer, F. (2003), *Broadband Dielectric Spectroscopy*, Springer, Heidelberg.

Kronig, R. (1926), On the theory of dispersion of X-rays, *J. Opt. Soc. Am. A*, *12*(6), 547–556.

Kupfer, K., E. Trinks, N. Wagner, and C. Hübner (2007), TDR measurements and simulations in high lossy bentonite materials, *Meas. Sci. Technol.*, *18*(4), 1118–1136.

Lauer, K., N. Wagner, and P. Felix-Henningsen (2010), Dielectric permittivity spectra of undisturbed soil samples from the taunus region, in *Proc. 1st European Conference on Moisture Measurement,*

Aquametry 2010, edited by K. Kupfer, pp. 500–510, MFPA Weimar, Weimar, Germany.

Lauer, K., N. Wagner, and P. Felix-Henningsen (2012), A new technique for measuring broadband dielectric spectra of undisturbed soil samples, *Eur. J. Soil Sci.*, *63*, 224–238.

Leroy, P., and A. Revil (2009), A mechanistic model for the spectral induced polarization of clay materials, *J. Geophys. Res.*, *114*, B10202, doi: 10.1029/2008JB006114.

Leroy, P., A. Revil, A. Kemna, P. Cosenza, and A. Ghorbani (2008), Complex conductivity of water-saturated packs of glass beads, *J. Colloid Interface Sci.*, *321*(1), 103–117.

Leroy, P., D. Jougnot, A. Revil, A. Lassin, and M. Azaroual (2012), A double layer model of the gas bubble/water interface, *J. Colloid Interface Sci.*, *388*(1), 243–256.

Levenberg, K. (1944), A method for the solution of certain problems in least squares, *Q. Appl. Math.*, *2*, 164–168.

Linard, Y., et al. (2011), Water flow in the Oxfordian and Dogger limestone around the Meuse/Haute-Marne Underground Research Laboratory, *Phys. Chem. Earth*, *36*(17), 1450–1468.

Logsdon, S., and D. Laird (2004), Cation and water content effects on dipole rotation activation energy of smectites, *Soil Sci. Soc. Am. J.*, *68*(5), 1586–1591.

Marquardt, D. (1963), An algorithm for least-squares estimation of nonlinear parameters, *J. Soc. Ind. Appl. Math.*, *11*(2), 431–441.

Mironov, V., M. Dobson, V. Kaupp, S. Komarov, and V. Kleshchenko (2004), Generalized refractive mixing dielectric model for moist soils, *IEEE Trans. Geosci. Remote Sens.*, *42*(4), 773–785.

Nicolson, A., and G. Ross (1970), Measurement of the intrinsic properties of materials by time domain techniques, *IEEE Trans. Insturm. Meas*, *IM-19*, 377–382.

Okay, G., P. Cosenza, A. Ghorbani, C. Camerlynck, J. Cabrera, N. Florsch, and A. Revil (2013), Localization and characterization of cracks in clay-rocks using frequency and time-domain induced polarization, *Geophys. Prospect.*, *61*(1), 134–152.

Olhoeft, G. (1974), Electrical properties of rocks, in *The Physics and Chemistry of Minerals and Rocks*, edited by R. G. J. Strens, pp. 261–278, John Wiley & Sons, London.

Oswald, B., J. Doetsch, and K. Roth (2006), A new computational technique for processing transmission-line measurements to determine dispersive dielectric properties, *Geophysics*, *71*(2), K31–K35.

Patnode, H., and M. Wyllie (1950), The presence of conductive solids in reservoir rocks as a factor in electric log interpretation, *J. Pet. Technol.*, *2*(2), 47–52.

Priesack, E., and W. Durner (2006), Closed-form expression for the multi-modal unsaturated conductivity function, *Vadose Zone J.*, *5*(1), 121–124.

Revil, A. (2013), Effective conductivity and permittivity of unsaturated porous materials in the frequency range 1 mhz–1ghz, *Water Resour. Res.*, *49*, 306–327, doi:10.1029/2012WR012700.

Revil, A., and N. Linde (2006), Chemico-electromechanical coupling in microporous media, *J. Colloid Interface Sci.*, *302*(2), 682–694.

Robinet, J.-C., P. Sardini, D. Coelho, J.-C. Parneix, D. Prêt, S. Sammartino, E. Boller, and S. Altmann (2012), Effects of mineral distribution at mesoscopic scale on solute diffusion in a clay-rich rock: Example of the Callovo-Oxfordian mudstone (Bure, France), *Water Resour. Res.*, *48*, W05554, doi:10.1029/2011WR011352.

Robinson, D. (2004a), Measurement of the solid dielectric permittivity of clay minerals and granular samples using a time domain reflectometry immersion method, *Vadose Zone J.*, *3*, 705–713.

Robinson, D., T. Kelleners, J. Cooper, C. Gardner, P. Wilson, I. Lebron, and S. Logsdon (2005), Evaluation of a capacitance probe frequency response model accounting for bulk electrical conductivity comparison with tdr and network analyzer measurements, *Vadose Zone J.*, *4*(4), 992–1003.

Robinson, D. A. (2004b), Calculation of the dielectric properties of temperate and tropical soil minerals from ion polarizabilities using the Clausius-Mosotti equation, *Soil. Sci. Soc. Am. J.*, *68*(5), 1780–1785.

Robinson, D. A., and S. P. Friedman (2003), A method for measuring the solid particle permittivity or electrical conductivity of rocks, sediments, and granular materials, *J. Geophys. Res.*, *108*(B2), 2076, doi:10.1029/2001JB000691.

Robinson, D. A., S. B. Jones, J. M. Wraith, D. Or, and S. P. Friedman (2003), A review of advances in dielectric and electrical conductivity measurement in soils using time domain reflectometry, *Vadose Zone J.*, *2*(4), 444–475.

Rotenberg, B., A. Cadene, J. Dufrêche, S. Durand-Vidal, J. Badot, and P. Turq (2005), An analytical model for probing ion dynamics in clays with broadband dielectric spectroscopy, *J. Phys. Chem. B*, *109*(32), 15,548–15,557.

Roth, K., R. Schulin, H. Fluhler, and W. Attinger (1990), Calibration of time domain reflectometry for water content measurement using a composite dielectric approach, *Water Resour. Res.*, *26*(10), 2267–2273.

Rowe, R., J. Shang, and Y. Xie (2001), Complex permittivity measurement system for detecting soil contamination, *Can. Geotech. J.*, *38*(3), 498–506.

Ryabov, Y., A. Gutina, V. Arkhipov, and Y. Feldman (2001), Dielectric relaxation of water absorbed in porous glass, *J. Phys. Chem. B*, *105*(9), 1845–1850.

Salat, C., and A. Junge (2010), Dielectric permittivity of fine-grained fractions of soil samples from eastern Spain at 200 MHz, *Geophysics*, *75*(1), J1–J9.

Sammartino, S., A. Bouchet, D. Prêt, J. Parneix, and E. Tevissen (2003), Spatial distribution of porosity and minerals in clay rocks from the Callovo-Oxfordian formation (Meuse/Haute-Marne, Eastern France)implications on ionic species diffusion and rock sorption capability, *Appl. Clay Sci.*, *23*(1), 157–166.

Santamarina, J. C., K. Klein, and M. Fam (2001), *Soils and Waves: Particulate Materials Behavior, Characterization and Process Monitoring*, Springer, Berlin Heidelberg, New York.

Savoye, S., J. Page, C. Puente, C. Imbert, and D. Coelho (2010), New experimental approach for studying diffusion through an intact and unsaturated medium: A case study with Callovo-Oxfordian argillite, *Environ. Sci. Technol.*, *44*(10), 3698–3704.

Schoen, J. H. (1996), *Physical Properties of Rocks: Fundamentals and Principles of Petrophysics*, Pergamon, Michigan.

Schwartz, R. C., S. R. Evett, M. G. Pelletier, and J. M. Bell (2009), Complex permittivity model for time domain reflectometry soil water content sensing: I. Theory, *Soil. Sci. Soc. Am. J.*, *73*(3), 886–897.

Shang, J., R. Rowe, J. Umana, and J. Scholte (1999), A complex permittivity measurement system for undisturbed/compacted soils, *ASTM Geotech. Test. J.*, *22*(2), 165–174.

Siggins, A., J. Gunning, and M. Josh (2011), A hybrid waveguide cell for the dielectric properties of reservoir rocks, *Meas. Sci. Technol.*, *22*(2), 025,702.

Skierucha, W., R. Walczak, and A. Wilczek (2004), Comparison of open-ended coax and TDR sensors for the measurement of soil dielectric permittivity in microwave frequencies, *Int. Agrophys.*, *18*(4), 355–362.

Slatyer, R. O. (1967), *Plant-Water Relationships*, Academic Press, New York.

Stillman, D., and G. Olhoeft (2008), Frequency and temperature dependence in electromagnetic properties of Martian analog minerals, *J. Geophys. Res.*, *113*, E09005, doi:10.1029/2007JE002977.

Topp, G. C., J. L. Davis, and A. Annan (1980), Electromagnetic determination of soil water content: Measurement in coaxial transmission lines, *Water Resour. Res.*, *16*(3), 574–582.

Vrugt, J. A., H. V. Gupta, W. Bouten, and S. Sorooshian (2003), A shuffled complex evolution metropolis algorithm for optimization and uncertainty assessment of hydrologic model parameters, *Water Resour. Res.*, *39*(1), 1201, doi:10.1029/2002WR001642.

Wagner, N., and K. Lauer (2012), Simultaneous determination of the dielectric relaxation behavior and soilwater characteristic curve of undisturbed soil samples, in *Geoscience and Remote Sensing Symposium (IGARSS), 2012 IEEE International*, Inst. of Mater. Res. & Testing, Bauhaus-Univ. Weimar, Weimar, Germany, pp. 3202–3205. IEEE.

Wagner, N., and A. Scheuermann (2009), On the relationship between matric potential and dielectric properties of organic free soils, *Can. Geotech. J.*, *46*(10), 1202–1215.

Wagner, N., E. Trinks, and K. Kupfer (2007a), Determination of the spatial TDR-sensor characteristics in strong dispersive subsoil using 3D-FEM frequency domain simulations in combination with microwave dielectric spectroscopy, *Meas. Sci. Technol.*, *18*(4), 1137–1146.

Wagner, N., K. Kupfer, and E. Trinks (2007b), A broadband dielectric spectroscopy study of the relaxation behaviour of subsoil, in *Proc. of the 7th International Conference on Electromagnetic Wave Interaction with Water and Moist Substances*, edited by S. Okamura, pp. 31–38, Institute of Material Research and Testing, Weimar.

Wagner, W., V. Naeimi, K. Scipal, R. Jeu, and J. Martinez-Fernandez (2007c), Soil moisture from operational meteorological satellites, *Hydrogeol. J.*, *15*(1), 121–131.

Wagner, N., A. Scheuermann, K. Kupfer, and E. Trinks (2009), Coupled hydraulic and dielectric material properties of soil, in *Proc. of the 8th Int. Conference on Electromagnetic Wave Interaction with Water and Moist Substances*, edited by P. Vainikainen, pp. 215–222, Picaset Oy, Helsinki, Finland.

Wagner, N., B. Müller, K. Kupfer, M. Schwing, and A. Scheuermann (2010), Broadband electromagnetic characterization of two-port rod based transmission lines for dielectric spectroscopy in soils, in *Proc. 1st European Conference on Moisture Measurement, Aquametry 2010*, edited by K. Kupfer, pp. 228–237, MFPA Weimar, Weimar, Germany.

Wagner, N., K. Emmerich, F. Bonitz, and K. Kupfer (2011a), Experimental investigations on the frequency and temperature dependent dielectric material properties of soil, *IEEE Trans. Geosci. Remote Sens.*, *47*(7), 2518–2530.

Wagner, N., M. Schwing, A. Scheuermann, F. Bonitz, and K. Kupfer (2011b), On the coupled hydraulic and dielectric material properties of soils: Combined numerical and experimental investigations, in *Proc. of the 9th International Conference on Electromagnetic Wave Interaction with Water and Moist Substances*, edited by D. B. Funk, pp. 152–161, ISEMA, Kansas City, MO, U.S.A.

Wagner, N., et al. (2013), Numerical 3D FEM and experimental analysis of the open-ended coaxial line technique for microwave dielectric spectroscopy on soil, *IEEE Trans. Geosci. Remote Sens.*, doi:10.1109/TGRS.2013.2245138, in press.

Weir, W. (1974), Automatic measurement of complex dielectric constant and permeability at microwave frequencies, *Proc. IEEE*, *62*(1), 33–36.

Wenk, H.-R., M. Voltolini, M. Mazurek, L. R. Van Loon, and A. Vinsot (2008), Preferred orientations and anisotropy in shales: Callovo-Oxfordian shale (France) and opalinus clay (Switzerland), *Clays Clay Miner.*, *56*(3), 285–306.

Winsauer, W., and W. McCardell (1953), Ionic double-layer conductivity in reservoir rock, *J. Pet. Technol.*, *5*(5), 129–134.